Accurate Image-Based Reconstruction of Non-Parametric Antenna EM-Simulation Models

Adrian Bekasiewicz[1[0000-0003-0244-541X]] and Remigiusz Martyniak[1[0009-0005-9337-1082]]

[1] Faculty of Electronics, Telecommunications and Informatics, Gdansk University of Technology, Narutowicza 11/12, 80-233 Gdansk, Poland
adrian.bekasiewicz@pg.edu.pl

Abstract. Development of new antennas is an inherently cognitive task that often involves re-use of structures from the literature, or their responses (e.g., for performance comparisons). The process might also be associated with reconstruction of their electromagnetic (EM) simulation models which—when performed manually—is both time-consuming and prone to errors. In this work, a proof-of-concept framework for image-based, non-parametric reconstruction of antenna EM models has been proposed. The method boils down to extraction of shape-related coordinates from photograph of a structure, followed by their processing and incorporation to a script that enables reconstruction and simulation of EM model. The approach has been demonstrated using two antennas.

Keywords: antenna reconstruction, computer-aided design, cost-efficient development, EM simulations, image-based processing.

1 Introduction

Design of modern antennas is an inherently cognitive process. It involves a mix of experience-driven topology development and its iterative tuning (preferably, using robust numerical algorithms). A fundamental challenge associated to identification of suitable topology w.r.t. specifications is lack of analytical, or empirical formulas that can govern the process. Instead, the development is an engineer in-the-loop procedure where geometry is iteratively altered and evaluated based on electromagnetic (EM) simulations [1]. In practice, new topologies are often derived through (more or less fundamental) modifications of baseline structures from the literature [2], [3]. Performance figures of literature-based antennas are also useful for benchmarks purposes [3]. Unfortunately, the required metrics might not always be accessible in the references [3], [4]. Furthermore, the reported ones are affected by the specifics of measurement, and/or simulation setups used for their determination, hindering unequivocal interpretation of data. The outlined difficulties can be alleviated by reconstructing the EM models of antennas from the literature.

Re-design of antenna from the literature is a time-consuming process. It typically involves identification of relevant parameters followed by reconstruction of all topological features of the radiator. The task can be hindered by inconsistencies between

ICCS Camera Ready Version 2026
To cite this paper please use the final published version:
DOI: 10.1007/978-3-032-29924-6_45

descriptions and visualizations of structures, as well as missing, or incorrect data on their dimensions. A counter-measure involves reverse-engineering of geometry based on analysis of available schematic illustrations and/or photographs [5]. Unfortunately, the process is not only tedious but also prone to errors.

Reconstruction of antennas from the literature can be performed using image processing techniques. For planar structures, the problem boils down to identification of geometry-specific coordinates from the image and their use to restore the EM model. The latter can be automated using appropriate scripts (supported by commercially available EM software) [5]-[8]. Image-based generation of antennas can be performed using machine learning (ML) techniques [7], [8]. In [7], a combination of convolutional neural network (CNN) and long-short-term memory (LSTM) models has been used for generation of parametric antenna models. A related concept, where processing of structures with complex antennas is realized using CNN-LTSM that maps a binary lattice onto the given topology has been proposed in [8]. Main limitation of the mentioned methods is that they require a large amount of labeled data for training of ML models. Furthermore, the predictive capabilities of ML models are limited to geometries that resemble reference data [7]. Given versatility of antennas from the literature (even when only variants of the given structure are considered [9]) the limitations of ML-based reconstruction are difficult to overcome. From this perspective, restoration of antenna EM models based on their images remains an open problem.

In this work, recreation of non-parametric EM models based on photographs of antenna prototypes has been proposed. The method does not rely on ML. Instead, it involves extraction of topology-specific coordinates based on identification of edges within a single photograph. The points also undergo de-noising, stratification (i.e., separation of individual polygons from the points), and reduction. The processed coordinates are fed to the script that automatically reconstructs EM model of the image-based radiator. The presented proof-of-concept framework has been demonstrated using two planar antennas. Discrepancy between frequency responses of the image-derived and reference EM models (in terms of resonance shift) does not exceed 2%.

2 Methodology

2.1 Problem Formulation

Let $\boldsymbol{I}$ be a grayscale image (M px × N px) of the antenna at hand. Also, let $I(x, y)$ be an element of $\boldsymbol{I}$ at x, y ($1 \le x \le M$, $1 \le y \le N$). EM model reconstruction involves three stages. First, a set $\boldsymbol{P} = \{\boldsymbol{p}_1, \ldots, \boldsymbol{p}_d\}$, $d = 1, \ldots, D$, of points $\boldsymbol{p}_d = [x_d, y_d]$ that represent edges from $\boldsymbol{I}$ is to be extracted. Next, a sequence of shapes (polygons) $\boldsymbol{S} = \{\boldsymbol{S}_1, \ldots, \boldsymbol{S}_o\}$, $o = 1, \ldots, O$, is to be sought, where each $\boldsymbol{S}_o \subset \boldsymbol{P}$ is the antenna building block. Note that $\boldsymbol{p}_{o.r} = [x_{o.r}\ y_{o.r}]$ ($x_{o.r} \le N$; $y_{o.r} \le M$) elements of each $\boldsymbol{S}_o = \{\boldsymbol{p}_{o.1}, \boldsymbol{p}_{o.2}, \ldots, \boldsymbol{p}_{o.r}\}$ are ordered to ensure that the extracted polygons do not self-intersect ($r < d$). Also, the points that constitute each $\boldsymbol{S}_o$ sequence are unique (i.e., they do not repeat between the extracted polygons). The last stage involves automatic generation of the script (a so-called macro) that describes the antenna to be restored, as well as reconstruction of the EM model and its simulation. The details concerning each step are given below.

ICCS Camera Ready Version 2026
To cite this paper please use the final published version:
DOI: 10.1007/978-3-032-29924-6_45

2.2 Image-Based Extraction of Antenna Coordinates

Extraction of edge coordinates based on image processing is a key component of the proposed framework. The algorithm is as follows [10]. Let $\boldsymbol{G}(\sigma)$ be an $\lambda \times \lambda$ matrix containing Gaussian kernel. Its $G(x, y, \sigma)$, $x, y \leq \lambda$, components are given as [10]:

$$G(x, y, \sigma) = \left(2\pi\sigma^2\right)^{-1} \exp\left(-\frac{x^2 + y^2}{2\sigma^2}\right) \tag{1}$$

where σ is user-defined; $\lambda = \lceil 6\sigma \rceil$ ("$\lceil \cdot \rceil$" denotes round-up to integer). Also, let $\boldsymbol{M} = (\boldsymbol{G}_x^{\,2} + \boldsymbol{G}_y^{\,2})^{0.5}$ and $\boldsymbol{\alpha} = \tan^{-1}(\boldsymbol{G}_y/\boldsymbol{G}_x)$ be a magnitude and direction of estimated edges (both $M \times N$) given gradients $\boldsymbol{G}_x = \boldsymbol{I}_G * \boldsymbol{S}_x$ and $\boldsymbol{G}_y = \boldsymbol{I}_G * \boldsymbol{S}_y$ ("$*$" is a convolution operator); $\boldsymbol{I}_G = \boldsymbol{I} * \boldsymbol{G}(\sigma)$ is a blurred input image, whereas $\boldsymbol{S}_x$ and $\boldsymbol{S}_y$ are Sobel filters [10]:

$$S_x = \begin{bmatrix} -1 & 0 & 1 \\ -2 & 0 & 2 \\ -1 & 0 & 1 \end{bmatrix}, S_y = \begin{bmatrix} -1 & -2 & -1 \\ 0 & 0 & 0 \\ 1 & 2 & 1 \end{bmatrix} \tag{2}$$

Edges within the image are found using non-maxima suppression [10]. Let d_k (k = 1, …, 4) be basic directions (angular orientations of edges w.r.t. x-axis in a Cartesian system). Also, let $\boldsymbol{\alpha}_1$ and $\boldsymbol{K}_1$ be 3 × 3 matrices extracted from $\boldsymbol{\alpha}$ and $\boldsymbol{M}$ around x_s, y_s ($x_s \leq M$, $y_s \leq N$ point). The values of nearest neighbors to $K_0 = M(x_s, y_s)$ are selected from $\boldsymbol{K}_1$ along $d_{\min} = d_k$ (i.e., an orientation with the smallest distance to $\boldsymbol{\alpha}_1$). The elements of non-maxima suppressed image $\boldsymbol{E}$ are set to $E(x_s, y_s) = 0$ when K_0 is smaller than the values for any of its neighbors; otherwise $E(x_s, y_s) = K_0$. Finally, matrices comprising so-called strong (true) and weak edges $\boldsymbol{E}_s$, $\boldsymbol{E}_w$ are identified. Their components are found as $E_s(x, y) = E(x, y) \geq t_h$, $E_w(x, y) = E(x, y) \geq t_l$ (t_l, t_h are user-defined); weak edge matrix is derived as $\boldsymbol{E}_w = \boldsymbol{E}_w - \boldsymbol{E}_s$. The weak edges are labeled as true provided their 8-connection to the strong ones, i.e., existence of a continuous path that connects weak-to-strong edge [10]. The elements of final matrix $\boldsymbol{E}^*$ are $E^*(x, y) = 1$ for each x, y pair corresponding to true edges; otherwise $E^*(x, y) = 0$. The set of extracted points $\boldsymbol{P}$—that correspond to indices of pixels from $\boldsymbol{E}^*$ for which $E^*(x, y) = 1$—undergoes further processing.

2.3 Coordinate-Based Polygons Extraction

A set of coordinates $\boldsymbol{P}$ is processed in multiple steps in order to identify non-intersecting polygons that constitute the antenna to be reconstructed. First the points are sorted. Let $\boldsymbol{p}^{(0)} \in \boldsymbol{P}^{(0)}$ be a left-lower corner from $\boldsymbol{P}^{(0)} = \boldsymbol{P}$. The sequence of points is initialized as $\boldsymbol{P}_S = \boldsymbol{p}^{(0)}$. At each step i (i = 1, …) the method identifies $\boldsymbol{p}^{(i+1)} = \text{argmin}(\|\boldsymbol{p}^{(i)} - \boldsymbol{p}_j\|)$, where $\boldsymbol{p}_j \in \boldsymbol{P}^{(i)}$ (j = 1, …, D–i) and $\boldsymbol{P}^{(i)} = \boldsymbol{P}^{(i-1)} \backslash \{\boldsymbol{p}^{(i)}\}$. Next, the point $\boldsymbol{p}^{(i+1)}$ is included at the end of sequence $\boldsymbol{P}_S = [\boldsymbol{p}^{(0)} \ldots \boldsymbol{p}^{(i)}\ \boldsymbol{p}^{(i+1)}]^T$ and the iteration index is increased as $i = i + 1$. The algorithm is terminated when $|\boldsymbol{P}^{(i)}| = 0$. Next, $\boldsymbol{P}_S$ is rotated to ensure its alignment with x-axis of the coordinate system. Let $\boldsymbol{P}_{R\text{tmp}}(\theta) = \boldsymbol{P}_S\boldsymbol{R}(\theta)$ represent coordinates rotated according to:

ICCS Camera Ready Version 2026
To cite this paper please use the final published version:
DOI: 10.1007/978-3-032-29924-6_45

$$\boldsymbol{R}(\theta)=\begin{bmatrix}\cos(\theta) & -\sin(\theta)\\ \sin(\theta) & \cos(\theta)\end{bmatrix}^{T} \tag{3}$$

Now, given that $\boldsymbol{P}_{R\text{tmp}}$ is an $D \times 2$ matrix of rotated x, y coordinates, i.e., $\boldsymbol{P}_{R\text{tmp}} = [\boldsymbol{X}_R{}^T \boldsymbol{Y}_R{}^T]$, let $\boldsymbol{p}_l = [\min(\boldsymbol{X}_R)\ \min(\boldsymbol{Y}_R)]$ and $\boldsymbol{p}_u = [\max(\boldsymbol{X}_R),\ \max(\boldsymbol{Y}_R)]$ be the corners that bound $\boldsymbol{P}_R$. The rotated coordinates are obtained by solving $\boldsymbol{P}_R = \text{argmin}(A(\boldsymbol{P}_{R\text{tmp}}(\theta)))$, where $A(\boldsymbol{P}_{R\text{tmp}}(\theta))$ is the area of the rectangle that bounds $\boldsymbol{P}_{Rtmp}$ according to $\boldsymbol{p}_l$ and $\boldsymbol{p}_u$. Next, $\boldsymbol{P}_N$ is obtained after unity-based normalization of $\boldsymbol{P}_R$. The sequence $\boldsymbol{P}_N = [\boldsymbol{p}_{N.1}\ \ldots\ \boldsymbol{p}_{N.D}]^T$ is then processed to remove noise (e.g., small groups of points separated from the remaining coordinates). Let $\boldsymbol{\delta} = [\delta_1\ \delta_2\ \ldots\ \delta_{D\text{-}1}]^T$ be the vector of distances between the consecutive points from $\boldsymbol{P}_N$. Also, let e_D and σ_D be the average and standard deviation of $\boldsymbol{\delta}$; $\boldsymbol{k} = [k_1\ \ldots\ k_{l1}\ \ldots\ k_{l2}\ \ldots\ k_L]^T$ ($l_1 < l_2 < L < D - 1$) is a vector with indices of points for which $\boldsymbol{\delta} > e_D + \sigma_D$. In other words, elements of $\boldsymbol{k}$ are indices that represent abnormal separation between points (i.e., indicate disjoint shapes). Now, let $\Delta k = [\Delta k_1\ \ldots\ \Delta k_{l1}\ \ldots\ \Delta k_{l2}\ \ldots\ \Delta k_{L\text{-}1}]$, where $\Delta k_l = k_{l+1} - k_l$ are lengths of separated groups of points $\boldsymbol{P}_{kl1} = [\boldsymbol{p}_{kl1+1}\ \boldsymbol{p}_{kl1+2}\ \ldots\ \boldsymbol{p}_{kl2-1}\ \boldsymbol{p}_{kl2}]^T$ (note that $|\boldsymbol{P}_{kl1}| = \Delta k_{l1} - 1$) between consecutive indices from $\boldsymbol{k}$ and $t_L = \beta(D-1)$ be threshold for minimum acceptable number of points in such groups (β is user-defined). The de-noised vector $\boldsymbol{P}_U$ comprises only $\boldsymbol{P}_{kl}$ groups for which the cardinality satisfies $|\boldsymbol{P}_{kl}| > t_L$ inequality. Next, $\boldsymbol{P}_U$ is separated into a set of sequences comprising individual shapes. The procedure is largely the same as the one outlined above. It involves calculation of $\boldsymbol{\delta}$ and identification of outlier indices $\boldsymbol{k}_0 = [k_{0.0}\ k_{0.1}\ \ldots\ k_{0.o\text{-}1}\ k_{0.o}]$, where $k_{0.0} = 1$ and $k_{0.o} = |\boldsymbol{P}_U|$. The oth shape separated from $\boldsymbol{P}_U$ is given as $\boldsymbol{S}_o = \{\boldsymbol{p}_{v1}, \boldsymbol{p}_{v2}, \ldots, \boldsymbol{p}_{vt\text{-}1}, \boldsymbol{p}_{vt}\}$, where $v_1 = k_{0.(o\text{-}1)}+1$, $v_2 = k_{0.(o\text{-}1)}+1$, $v_{t\text{-}1} = k_{0.o}-1$, and $v_t = k_{0.o}$, respectively. The set comprising all sequences is given as $\boldsymbol{S} = \{\boldsymbol{S}_1, \ldots, \boldsymbol{S}_o\}$.

Finally, lengths of $\boldsymbol{S}_o$ sequences are reduced while preserving the retained shape. The goal here it to scale down irregularities resulting from image-based edge detection in order to ensure manageable simulation cost (discretization of uneven edges is subject to increased mesh density, which negatively affects the cost of EM simulations). To simplify the notation, let $\boldsymbol{Q} = \boldsymbol{S}_o$ be an ordered sequence of points that represent oth polygon such that $\boldsymbol{Q} = \{\boldsymbol{q}_1, \ldots \boldsymbol{q}_K\}$, where $K = |\boldsymbol{Q}|$. Then, let $\boldsymbol{\Psi}$ be a set that contains selected subsequences of $\boldsymbol{Q}$. The algorithm is as follows [11]:

1. Set $\boldsymbol{\Psi} = \{\boldsymbol{Q}\}$, $I = |\boldsymbol{\Psi}|$, $i = 1$, $\boldsymbol{P}_{\text{out}} = \{\boldsymbol{q}_1, \boldsymbol{q}_K\}$, and $\boldsymbol{\Psi}_{\text{tmp}} = \{\}$;
2. Select $\boldsymbol{Q}_i \subset \boldsymbol{\Psi}$ and set $K = |\boldsymbol{Q}_i|$;
3. Calculate $\boldsymbol{\delta}_i$, i.e., a vector of perpendicular distances of $\boldsymbol{q}_{i.k} \in \boldsymbol{Q}_i$ points ($k = 2, \ldots, K$–1) to a line segment defined by $\{\boldsymbol{q}_{i.1}, \boldsymbol{q}_{i.K}\} \subset \boldsymbol{Q}_i$ pair;
4. Calculate $\delta_{\max} = \max(\boldsymbol{\delta}_i)$; If $\delta_{\max} < \varepsilon$ go to 6; otherwise set $k_{\max}$ as index of $\delta_{\max}$ in $\boldsymbol{\delta}_i$ and go to Step 5;
5. Set $\boldsymbol{P}_{\text{out}} = \boldsymbol{P}_{\text{out}} \cup \boldsymbol{q}_{i.k\max}$, $\boldsymbol{Q}_{i1} = \{\boldsymbol{q}_{i.1}, \ldots, \boldsymbol{q}_{i.k\max}\}$, $\boldsymbol{Q}_{i2} = \{\boldsymbol{q}_{i.k\max}, \ldots, \boldsymbol{q}_{i.K}\}$, $\boldsymbol{\Psi}_{\text{tmp}} = \boldsymbol{\Psi}_{\text{tmp}} \cup \{\boldsymbol{Q}_{i1}, \boldsymbol{Q}_{i2}\}$;
6. If $i = I$, go to Step 7; otherwise, set $i = i + 1$ and go to step 2;
7. If $\boldsymbol{\Psi} = \{\}$, set $\boldsymbol{S}^* = \boldsymbol{P}_{\text{out}}$ and END; otherwise reorder sequences from $\boldsymbol{\Psi}_{\text{tmp}}$ by their descending lengths, set $\boldsymbol{\Psi} = \boldsymbol{\Psi}_{\text{tmp}}$, $i = 1$, $I = |\boldsymbol{\Psi}|$ and go to Step 2.

Upon termination $\boldsymbol{S}_o = \boldsymbol{S}^*$ is set. The tolerance threshold ε is user-defined. Sequence for which all $\boldsymbol{\delta}_i$ distances are below the threshold are not considered for fur-

ICCS Camera Ready Version 2026
To cite this paper please use the final published version:
DOI: 10.1007/978-3-032-29924-6_45

ther processing, hence $\boldsymbol{\Psi} = \{\}$ is equivalent to reduction of all sequences. The routine is executed for all $\boldsymbol{S}_o \subset \boldsymbol{S}$ polygons.

The coordinate-based polygons extraction procedure described above can be summarized as follows:

1. Extract $\boldsymbol{P}_S$, i.e., a sorted matrix of coordinates from $\boldsymbol{P}$;
2. Generate $\boldsymbol{P}_R$ through rotation of $\boldsymbol{P}_S$; normalize $\boldsymbol{P}_R$ obtain $\boldsymbol{P}_N$;
3. Obtain $\boldsymbol{P}_U$ by distance-based de-noising of $\boldsymbol{P}_N$;
4. Separate $\boldsymbol{P}_U$ into $\boldsymbol{S}_1$, $\boldsymbol{S}_2$, …, $\boldsymbol{S}_o$ and perform reduction of polygons.

Upon processing, the set $\boldsymbol{S}$ can be used to reconstruct the antenna structure.

2.4 Reconstruction of Antenna EM Model

Feasibility of the antenna EM model is subject to availability of substrate with straight edge. The latter is necessary to accommodate a reference point for excitation of the driven element (i.e., the radiator) through a waveguide port while maintaining consistency of mesh [12]. Unfortunately, polygons $\boldsymbol{S}_o \subset \boldsymbol{S}$ might not fulfill the mentioned requirement. This is due to the noise associated with determination of edges using algorithm of Section 2.2, as well as challenges related to separation of antenna feed from the outline (substrate) based on evaluation of outliers as explained in Section 2.3. In this work, the problem is addressed using a bounding box $\boldsymbol{P}_B$ generated w.r.t. $\boldsymbol{S}_o$ with the largest area. The procedure involves uniform scaling of the box to $\boldsymbol{P}_{BS} = \gamma\boldsymbol{P}_B$ (here, $\gamma = 0.995$ is used) followed by generation of $\boldsymbol{S}_{B.o} = \boldsymbol{S}_o \setminus \boldsymbol{P}_{BS}$ for all o shapes; if $\boldsymbol{S}_{B.o} = \{\}$, then $\boldsymbol{S}_{B.o} = \boldsymbol{P}_{BS}$ is used which defines the substrate for antenna generation (see Fig. 1 for conceptual illustration). Next, the modified shapes are scaled according to measured dimensions of the prototype $x_{\max}$, $y_{\max}$ (both user-defined) to obtain the final set $\boldsymbol{S}_F = \{\boldsymbol{S}_{F.1}, \ldots, \boldsymbol{S}_{F.o}\}$ that represents individual layers of the antenna geometry. Finally, each of $\boldsymbol{S}_{F.o}$ shapes is labeled according to its function (i.e., substrate, metal, cutout; the list of ordered labels is given as $\boldsymbol{L} = \{L_1, L_2, \ldots\}$) and position w.r.t. the substrate side $\boldsymbol{Z} = \{Z_1, Z_2, \ldots\}$. Note that the parameters can be set either to 0 or h, *i.e.*, bottom or top. Moreover, a coordinate point $\boldsymbol{p}_f = [x_f\, y_f]$ that represents location of the port for structure excitation is obtained based on analysis of coordinates from $\boldsymbol{S}_{F.o}$ that are located on the edge of shape labeled as substrate.

Once $\boldsymbol{S}_F$ and $\boldsymbol{p}_f$ are obtained, the antenna EM model can be reconstructed using automatically generated script. Inputs for the latter include substrate properties, i.e., permittivity ε_r, thickness h, loss tangent $\tan(\delta)$, as well as metal thickness T, and frequency range [6]. EM model generation involves iterative processing of $\boldsymbol{S}_{F.o} \subset \boldsymbol{S}_F$ shapes followed by determination of appropriate operations between them (e.g., subtraction) based on appropriately ordered lists of labels $\boldsymbol{L}$ and substrate-related orientations $\boldsymbol{T}$. The routine can be summarized as follows:

1. Generate EM solver configuration and substrate properties based on provided list of input parameters;
2. Define substrate brick based on $\boldsymbol{S}_{F.1}$ and thickness h; set $l = 2$;
3. If $l \leq O$ and L_l indicates "metal", go to Step 4; if $l \leq O$ and L_l indicates "cutout", go to Step 5; otherwise, go to Step 7;

ICCS Camera Ready Version 2026
To cite this paper please use the final published version:
DOI: 10.1007/978-3-032-29924-6_45

4. Generate a polygon brick defined by $\boldsymbol{S}_{F.l}$ at Z_l plane on the substrate and set $l = l + 1$ and go to Step 3;
5. Generate a polygon brick defined by $\boldsymbol{S}_{F.l}$ at Z_l plane on the substrate;
6. Find index $1 < l_1 < l$ that identifies "metal" polygon $\boldsymbol{S}_{F.l1}$ which overlaps with $\boldsymbol{S}_{F.l}$ shape; define subtraction operation, set $l = l + 1$ and go to Step 3;
7. Generate microwave port according to the given $\boldsymbol{p}_f$ point and END.

It should be noted that generation of macros that support configuration of solver, definition of substrate, frequency range, shapes (polygons), as well as operations between the shapes are well explained in the documentation of EM simulation packages (here, CST Studio [12]). Having that in mind, discussion of specific functions and their syntax are beyond the scope of this work. It is worth mentioning, however, that the above outlined routine is configured to generate macros in Basic programming language which is supported by CST Studio package [12].

Finally, the generated macro can be used to generate the EM model of the image-based antenna and execute its simulation to obtain $\boldsymbol{R}(\boldsymbol{S})$ response. All of the outlined routines have been implemented in Python. Conceptual illustration of the proposed framework is shown in Fig. 2. It should be reiterated that the presented method involves an end-to-end processing of only one image, which is fundamentally different when compared against ML-based techniques of [7], [8].

3 Results

The proposed framework has been validated based on two manufactured planar antennas. Upon reconstruction, performance figures of the radiators are evaluated using the same simulation settings as for the models used for fabrication of prototypes.

Consider a rectangular patch implemented on AD255C substrate (cf. Fig. 3; h = 1.5 mm). The image (868 px × 1205 px) processing is performed using the algorithm of Section 2. The user-defined parameters are $\{\sigma, t_h, t_l, \beta, \varepsilon, x_{\max}, y_{\max}\}$ = {0.5, 1.2, 0.4, 0.01, 0.003, 46.95, 33.77}; $x_{\max}$, $y_{\max}$ (in mm) are measured using a caliper. The number of points that represent the extracted structure is only 21 (from initial 4584). The antenna EM model comprises 79,000 mesh cells (vs. 62,800 for the reference design). Reflection responses for the reference and regenerated models are compared in Fig. 4. The discrepancy between shapes—here, a median distance between points from image-based and reference geometries—is just 0.1 mm. The resonance shift of the reconstructed response is 20 MHz, or just 0.5% w.r.t. the 4.1 GHz center frequency for the reference model, which also emphasizes high similarity between the geometries.

The second image (1163 px × 931 px) comprises a tri-band dipole on a RO4358B substrate (h = 0.76 mm; cf. Fig. 3) [2]. The radiator is excited through a coplanar line (with narrow gaps between the feed and ground plane) which makes its reconstruction challenging. Except for the substrate size (here, $x_{\max}$ = 51.17 mm, $y_{\max}$ = 33.55 mm), the algorithm settings are the same as for the patch. The initial number of coordinates is reduced from 10743 to 381. Nonetheless, the recreated model features 2.5-fold denser mesh (325,600 cells) w.r.t. the reference one (124,600). As shown in Fig. 4, reflection responses obtained for both EM models are similar. Maximum shift of res-

ICCS Camera Ready Version 2026
To cite this paper please use the final published version:
DOI: 10.1007/978-3-032-29924-6_45

onances is 100 MHz, or just 1.8% relative to 5.3 GHz (the third frequency of operation). A distance between geometries (shape-wise) is around 0.4 mm.

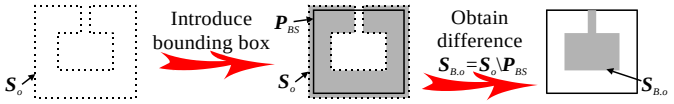

Fig. 1. The use of scaled-down bounding box (—) and difference operation to refine a point-based (⋯) polygon (gray) that incorrectly blends the substrate and outline of the radiator.

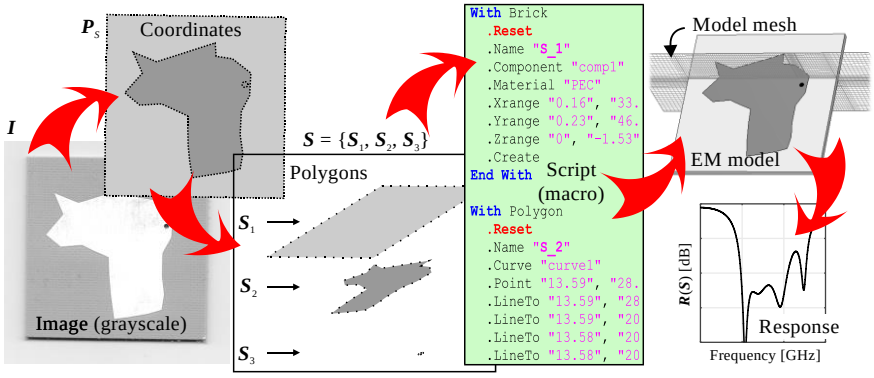

Fig. 2. Image-based reconstruction of antenna EM model: conceptual illustration of the proposed framework with highlight on the key post-processing steps.

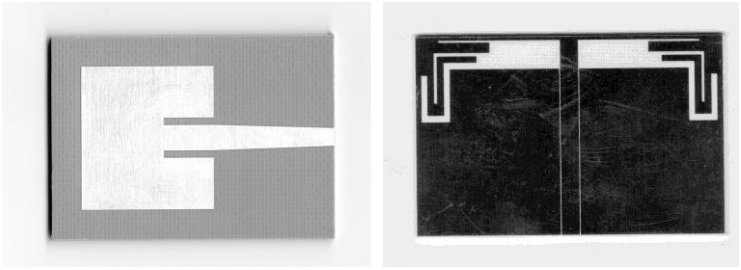

Fig. 3. Photographs of the example antennas: microstrip patch (left) and tri-band dipole (right).

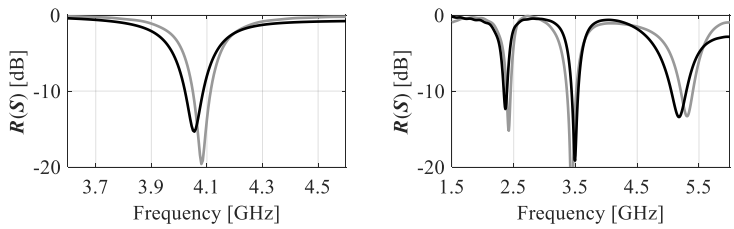

Fig. 4. Reflection responses obtained for the original (gray) and reconstructed from images (black) antenna EM models for: patch radiator (left) and tri-band dipole (right).

ICCS Camera Ready Version 2026
To cite this paper please use the final published version:
DOI: 10.1007/978-3-032-29924-6_45

4 Conclusion

In this work, a proof-of-concept framework for non-parametric reconstruction of antenna EM simulation models based on images of their manufactured prototypes has been proposed. The method involves several processing steps that include identification and conversion of edges to coordinates, as well as their de-noising, stratification, reduction and scaling. The obtained points are fed to automatically generated scripts that reconstruct the EM model of antenna at hand and enable its simulation. The approach has been demonstrated using two planar radiators. High resemblance between the reference and reconstructed models has been achieved. The performance discrepancy (expressed in terms of resonances shift) does not exceed 2%. Dissimilarity of geometries (shape-wise) is also maintained below 0.5 mm.

Future work will focus on streamlining the geometry extraction procedure, as well as its extension to handle more complex microwave geometries and dual-layer components. Parametric reconstruction of topologies will also be considered.

Acknowledgments. This work was supported in part by the National Science Center of Poland Grant 2021/43/B/ST7/01856.

Disclosure of Interests. The author declares no conflicts of interests.

References

1. Koziel, S., Ogurtsov, S.: Antenna design by simulation-driven optimization. Springer, (2014)
2. Bekasiewicz, A., Koziel, S.: Miniaturized uniplanar triple-band slot dipole antenna with folded radiator. Microwave Opt. Tech. Lett. **60**(2), 386–389 (2018)
3. Khan, M.S., *et al.*: A compact CSRR-enabled UWB diversity antenna. IEEE Ant. Wireless Prop. Lett. **16**, 808–812 (2017)
4. Haq, T., Koziel, S.: Novel complementary multiple concentric split ring resonator for reliable characterization of dielectric substrates with high sensitivity. IEEE Sens. J. **24**(10), 16233–16241 (2024)
5. Jacobs, J.P.: Accurate modeling by CNN regression of resonant frequencies of dual-band pixelated microstrip antenna. IEEE Ant. Wireless Prop. Lett. **20**(12), 2417–2421 (2021)
6. Bekasiewicz, A., *et al.*: Strategies for feature-assisted development of topology agnostic planar antennas using variable-fidelity models. J. Comp. Sci. **85**, 102521 (2025)
7. Wei, Z., *et al.*: Fast and automatic parametric model construction of antenna structures using CNN–LSTM networks. IEEE Trans. Ant. Prop. **72**(2), 1319–1328 (2024)
8. Zhu, Z., Tian, Y., Sun, J.: Antenna modeling based on image-CNN-LSTM. IEEE Ant. Wireless Prop. Lett. **23**(9), 2738–2742 (2024)
9. Bekasiewicz, A., Koziel, S.: Structure and computationally efficient simulation-driven design of compact UWB monopole antenna. IEEE Ant. Wireless Prop. Lett. **14**, 1282–1285 (2015)
10. Gonzalez R.C., Woods R.E.: Digital Image Processing. 4th ed. Pearson, New York, (2018)
11. Shi, W., Cheung, C.K.: Performance evaluation of line simplification algorithms for vector generalization. Cartographic J. **43**(1), 27–44 (2006)
12. CST Microwave Studio, Dassault Systems, 10 rue Marcel Dassault, CS 40501, Vélizy-Villacoublay Cedex, France, (2019)

ICCS Camera Ready Version 2026
To cite this paper please use the final published version:
DOI: 10.1007/978-3-032-29924-6_45